35-GHz Dual-Polarization Propagation Link for Rain-Rate Estimation

CHRISTOPHER S. RUF, KULTEGIN AYDIN, SAVYASACHEE MATHUR, AND JUSTIN P. BOBAK

Department of Electrical Engineering, The Pennsylvania State University, University Park, Pennsylvania

(Manuscript received 5 April 1995, in final form 15 August 1995)

ABSTRACT

A 35-GHz dual-polarization propagation link (DPPL) is described and initial measurements are presented. The instrument is essentially a small, low-power, portable, dual linearly polarized pulsed radar that provides differential attenuation measurements along a short propagation path in rain. Alternate vertically and horizontally polarized pulses are transmitted at a 2200-Hz pulse repetition frequency (PRF). Rain attenuation measurements are made by range gating a passive corner reflector located some distance from the DPPL. Deployment logistics are considerably simplified relative to a standard unidirectional propagation link.

Using the ratio of horizontal to vertical received power to determine the differential attenuation reduces the sensitivity to instrument fluctuations since transmitter and receiver drifts slower than the PRF will be cancelled out. This greatly relaxes the calibration and stability requirements on the hardware. Simultaneous measurements of differential attenuation in rain by the DPPL and of rainfall rate with a ground-based rain gauge demonstrate the feasibility of this technique.

1. Introduction

There is a clear need on the part of the hydrological remote sensing community for the capability to measure spatially averaged rain rate with both high precision over short timescales and long-term absolute accuracy. For example, ground truth validation has been identified as a key requirement of the science effort associated with NASA's Tropical Rainfall Measuring Mission (TRMM) (NASA 1994). This will require a ground truth capability for spatially averaged measurements on short timescales in order to reduce the temporal and spatial decorrelation uncertainties inherent in satellite–surface intercomparisons. Long-term accuracy on the part of the ground systems is also desirable in order to monitor TRMM performance over the course of the mission. In both respects, the DPPL should be a useful tool for validation of the instantaneous 4 km × 4 km spatially averaged measurements by the TRMM precipitation radar. As another example, the measurement of spatially averaged rain accumulation over longer timescales, but with very stable absolute calibration, is an important component of global climate monitoring over the tropical oceans due to the scarcity of surface meteorological radars there. Here an important design consideration is the ease (and cost) of deploying a network of instruments at numerous remote island sites. The 35-GHz dual-polarization propagation link (DPPL) presented here provides all of these capabilities in a small, highly portable, easily deployed, and relatively inexpensive package. It should be a valuable supplement to the existing network of surface radars in the Tropics. The DPPL will also be useful as a source of information about the basic spatial and temporal variability of rainfall over 100-m to 1-km scales.

Conventional unidirectional microwave propagation links typically use a transmitter instrument at one end of the link and a receiver at the other end. Both ends of the link require power and a controlled environment to protect the instruments and to stabilize the sensitive electronics. The receiver end is generally located higher above the ground in order to eliminate multipath effects. The receiver also usually includes a data acquisition system and some form of data communication. In the case of the DPPL, the transmitter and receiver are housed in a single enclosure that can be located near ground level without significantly compromising performance. Power, environmental control, and data communication are only needed at the instrument end of the link. A passive corner reflector is deployed at the other end with a simple open-sided tarp for protection. The tarp is large enough to keep the corner reflector dry during rain, maintaining its differential radar cross section. Best link performance is achieved with the corner reflector elevated at least a beamwidth up above the ground clutter, similar to the receiver end of a unidirectional link. However, the fact that the corner reflector is passive can greatly simplify this deployment requirement.

Corresponding author address: Prof. Christopher S. Ruf, Department of Electrical Engineering, The Pennsylvania State University, 121 Electrical Engineering East, University Park, PA 16802-2705.

© 1996 American Meteorological Society

2. Theory—Average and differential attenuation

The relation between microwave specific attenuation A and rainfall rate R is nearly linear near 35 GHz (Ryde 1947; Wexler and Atlas 1963). Based on this, experiments have been performed in the past, some with success, to estimate path-integrated R from the measurement of A at 35 GHz (Collis and Ligda 1961; Godard 1965; Harrold 1967). More recently, Atlas and Ulbrich (1977) explained the reasons for the linear relationship between R and A at this frequency. They noted the insensitivity to temperature and also the insensitivity to variations in the raindrop size distribution, and suggested using A_h or A_v to determine rain rate, where h and v correspond to horizontal and vertical polarizations, respectively. They found the relationship between horizontal or vertical A (dB km^{-1}) and R (mm h^{-1}) to be nearly linear as

$$A = 0.228R \tag{1}$$

under the assumption of spherical raindrops. In practice, some scatter in this relation will result due to variations in the ellipticity of the nonspherical raindrops with size. Atlas and Ulbrich (1977) also suggested using polarization to compensate for the change in drop shape and canting angle variations over the propagation path. They found linear relationships as

$$A_{\text{avg}} = 0.5(A_h + A_v) = 0.22R \tag{2}$$

$$\Delta A = A_h - A_v = 0.039R. \tag{3}$$

Since the average specific attenuation A_{avg} produces a more enhanced signal, they suggest its use for estimating R, rather than the differential specific attenuation, ΔA. Jameson (1991) also suggested the use of A_{avg} to estimate rain rate due to its relative independence of drop shape. Although the sensitivity of ΔA to rain rate is considerably lower than that of A itself, we believe that the additional measurement stability inherent in the differential data processing is an important mitigating factor in its favor. In addition, differential measurements will cancel the second-order effects of polarization-independent attenuation along the link path, for example, due to oxygen, water vapor, or mist. We note here that a number of millimeter-wave propagation links have been built in the past (Wallace 1988), but none to our knowledge have utilized the differential attenuation relationship.

There are opposing views regarding the effects of multiple scattering due to rain on signal propagation. According to Crane (1971), multiple scattering will reduce the attenuation in incoherent transmission systems; this effect would become significant along paths in heavier rainfall and at microwave frequencies above 20 GHz. Hogg and Chu (1975), on the other hand, argue that multiple scattering along microwave transmission paths is negligible even at rainfall rates of 100 mm h^{-1} due to the sparseness in mean spacing of raindrops compared to a wavelength. As a result, it is unclear at this time what the effects of multiple scattering will be on the measurement of ΔA. This indicates the need for further analysis of the problem.

3. Description of DPPL instrument

The operating principle of this instrument is essentially that of a dual linearly polarized pulsed radar. A block diagram of the instrument is shown in Fig. 1. A summary of its operating characteristics are given in Table 1. A more detailed description of the DPPL is available in Mathur (1994). The 35-GHz RF source is provided by a phase-locked Gunn oscillator producing +23 dBm of power. The source is pulsed by a PIN diode SPST switch. The PIN switch features 10-ns off-to-on and 40-ns on-to-off settling times, which effectively limit the minimum transmit pulse width to about

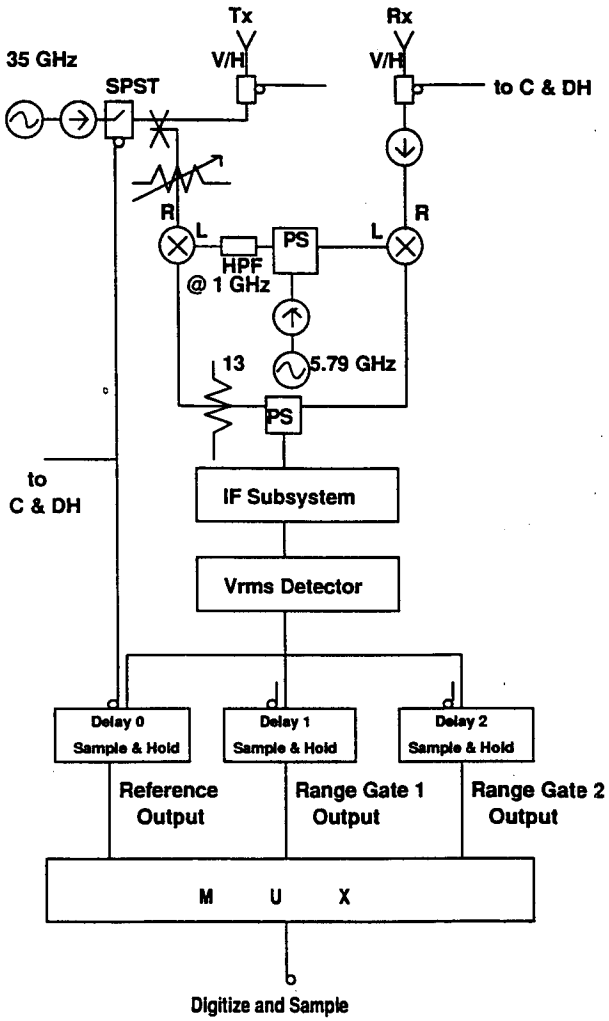

FIG. 1. Block diagram of the 35-GHz dual-polarization propagation link (DPPL).

TABLE 1. The 35-GHz dual-polarization propagation link operating characteristics.

Transmit frequency (GHz)	35.00
Transmit power at antenna (dBm)	21.0
Antenna type (Tx and Rx)	30-cm Gaussian lens loaded horns
Tx and Rx antenna gain (dBi)	39.0
Tx and Rx antenna HPBW (°)	2.3
Polarization type	linear V or H, selectable
Polarization select settling time (μs)	80
Polarization switching speed (Hz)	2200
Transmit pulse width (ns)	80–300, selectable
Receiver noise figure (dB)	21
Receiver predetection bandwidth (MHz)	10–150, selectable

80 ns. Polarization switching is achieved using a commercial (Alpha Industries) Faraday rotation solenoid immediately before the transmit antenna. The large inductance of the solenoid coil has a significant effect on the settling time of the transition from one to the other linearly polarized state. The settling time of 80 μs effectively limits the maximum transmit pulse repetition frequency (PRF) to about 2200 Hz, since the polarization is alternated between pulses. The transmit antenna is a 30-cm Gaussian lens loaded horn with a half-power beamwidth of 2.3°. Rain-attenuation measurements are made by placing a corner reflector in the main beam of the antenna. A separate receive antenna, identical to and coaligned with the transmit antenna and also followed by a similar polarization switch, is located several inches from the transmitter. It sends the signal to the receiver.

The receiver section includes one stage of down conversion, to an IF of 250 MHz, which is obtained using a sixth-harmonic mixer pumped by a free-running, temperature-stabilized 5.7917-GHz dielectric resonant oscillator. This method of down conversion offers a considerable savings in cost but results in a fairly high (21 dB) receiver noise figure that would be unacceptably high in many pulsed radar applications. However, this is a propagation link that uses a large corner reflector as its target, which allows this approach to be used with a satisfactory margin in signal to noise. Gain and power detection are performed at the first IF stage. Range gating, analog data sample-and-hold, analog-to-digital conversion, and digital data buffering are all performed by a commercial (Stanford Research Systems) radar controller. Final data storage and overall system control are provided by a 486DX-class personal computer.

The instrument is packaged in a single container measuring 100 cm × 50 cm × 70 cm. The antennas are mounted beside one another on a 100 cm × 50 cm face, with precision alignment and pointing adjustments included in the mounting hardware. This container weighs 60 kg. In addition, the system requires a support 19″ rack mount enclosure that houses the computer control, pulse generation and range gating, data acquisition, and power supply subsystems. The rack mount enclosure weighs 35 kg. Two trihedral corner reflectors are currently available, both with mounting hardware to permit precision pointing. A 15-cm reflector (RCS = 29 m^2 at 35 GHz) is used for link ranges of order 100 m. A 46-cm reflector (RCS = 2444 m^2 at 35 GHz) is used for link ranges of order 1000 m.

4. Demonstration of instrument stability

The stability of the DPPL instrument has been tested with the intent of quantifying the benefits of using a differential measurement technique. Measurement of the attenuation through rain at a single linear polarization, A_h or A_v, can result in an estimate of the rain rate that is sensitive to instrument instability. For example, a decrease in the transmitter power or the receiver gain would lower the detected power and could be erroneously interpreted as an increase in the rain rate. Single-polarization measurements are also subject to nonspherical drop-shape-dependent uncertainty, as discussed above. Measurement of the polarization averaged attenuation A_{avg} will correct for much of the drop shape uncertainty but will still be susceptible to instrument instabilities. It is expected that the differential measurement ΔA will be largely free of instrument-instability-induced effects, provided the instabilities occur on timescales significantly longer than the 0.5-ms switching time between alternate vertically and horizontally polarized pulses. Of course, the sensitivity of A_{avg} to rain rate is approximately five times greater than that of ΔA [see (2) and (3)]. Therefore, the stability of the differential measurements will need to be more than five times better in order to retrieve rain rate more reliably.

Preliminary data from these stability tests were first presented by Ruf et al. (1994). The results presented here represent additional processing of a larger dataset, together with a more complete discussion of the measurement procedure and the data processing. A continuous 81-h time series of data was recorded in clear weather with the DPPL deployed at a height of 20 m on the roof of a building at University Park, Pennsylvania. The 46-cm corner reflector was located 255 m away on the catwalk of a brick chimney, also at a height of 20 m. The DPPL was operated with a PRF of 2200 Hz and a pulse width of 240 ns. The line of sight path between the DPPL and corner reflector was unobstructed. The 2200-Hz PRF produces 1100 interleaved vertical and horizontal samples every second. The 1-s averages of the individual horizontal and vertical received powers, P_h and P_v, respectively, were recorded every 5 s for the 81-h period.

An assessment of the short-term stability of the processed data is made by estimating the standard devia-

tion of the samples when smoothed by a running average of variable time length. The averaging time is varied in multiples of the unit sampling rate of 5 s. The standard deviation is first estimated from consecutive sets of three smoothed samples. Each set of three samples provides one noisy estimate of the true standard deviation. This collection of noisy estimates is then averaged together, resulting in a single mean estimate of the standard deviation. For example, the 81-h time series produced approximately 24 000 samples of P_h, one every 5 s. To determine the standard deviation of samples smoothed by 50 s of averaging, consecutive sets of 10 samples are averaged together, resulting in 2400 smoothed samples of P_h. Each consecutive set of three of these samples is used to compute an unbiased estimate of the standard deviation, resulting in 800 estimates. These 800 estimates are then averaged together. This type of processing provides a good measure of the short-term variability of the samples. If a single standard deviation were computed directly from the complete set of 2400 smoothed samples in the above example, both short-term variations and longer-term drifts would be included in the resulting statistic. The running average was varied from no averaging (samples every 5 s) up to about 500 min.

The results of this stability test are shown in Figure 2. The standard deviation of the received power is plotted in Fig. 2a versus the smoothing time for the measurements of $P_{\text{avg}} = 0.5(P_v + P_h)$ and $\Delta P = P_v/P_h$, which would respectively be used to estimate A_{avg} and ΔA. (The behavior of P_h and P_v individually were very similar to that of P_{avg}.) In both cases, the standard deviation should decrease with smoothing time as long as the measurement noise is stationary and the measurement mean is constant. In the case of P_{avg}, the standard deviation continues to drop up to time averages of about 1 min, then flattens out at a level of 0.1 dB and begins to rise again for time averages above 4 min. This indicates that the absolute levels of instrumental and/or clutter biases are well correlated over time periods of less than 1–2 min. At very large time averages, the estimate of the standard deviation becomes somewhat noisy since fewer independent samples are available with this much averaging. However, the standard deviations are clearly much larger on these timescales—of the order of 1 dB—and indicate the rms level of long term drifts in the DPPL hardware.

Figure 2a also shows the short-term stability of ΔP. Polarization switching is operated at 2200 Hz, so polarization-independent drifts in the instrumental and/or clutter biases that occur more slowly than approximately 0.5 ms are largely cancelled out. The standard deviation monotonically decreases with smoothing time up to about 60 min, then increases slightly beyond that. The standard deviation is in the range 0.006–0.009 dB for averaging times between 20 and 500 min.

The stability of the rain-rate estimates corresponding to these standard deviations can be determined by scaling the values according to (2) and (3). The results are shown in Fig. 2b. On timescales of less than about 5 min, P_{avg} is seen to more precisely estimate rain rate because of its higher sensitivity. Beyond 5 min, however, the differential processing is clearly superior. These results can be interpreted in several ways. Figure 2b can be considered a noise limit on the ability of the DPPL to resolve the temporal spectral variability of the rain-rate process. This type of analysis would be concerned more with rain-rate variability than with absolute rain accumulation. The hardware-dependent absolute accuracy of the DPPL's retrieval of rain rate, on the other hand, is better estimated from the standard deviations shown in Figure 2b at the longest integration times. For example, drifts of 1–2 dB in P_{avg} from day to day and week to week were commonly observed, as

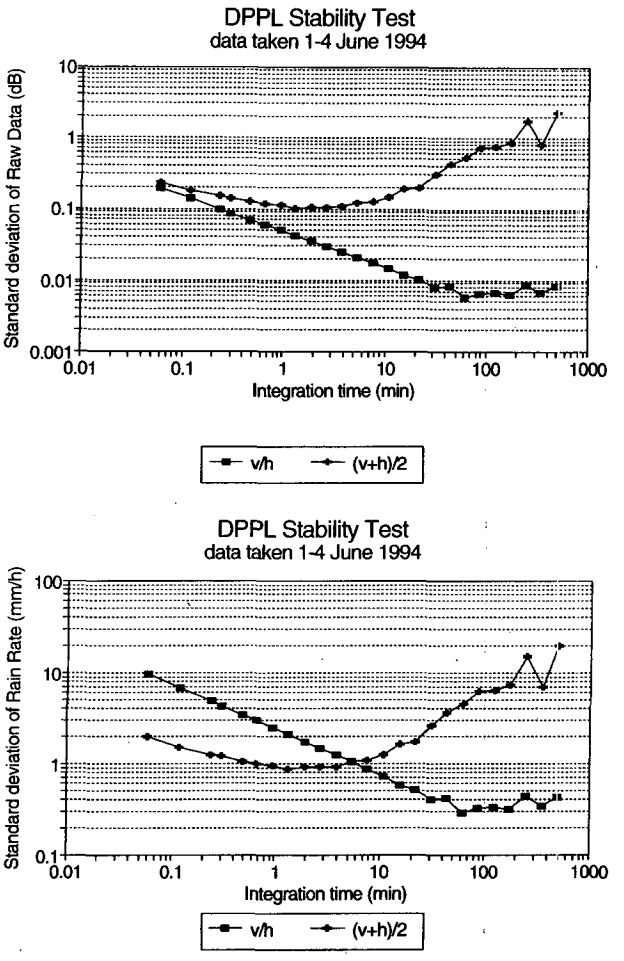

FIG. 2. Short-term stability characteristics of the DPPL using averaged [$(v + h)/2$] and differential (v/h) polarization processing. (a) Standard deviation of the received power over a 255-m link path for varying lengths of data integration time. (b) Standard deviation of the corresponding estimates of rain rate. Note that on the longer timescales, most of the noise and clutter fluctuations have been cancelled out by the differential processing, whereas the average received power is still sensitive to instrument drifts.

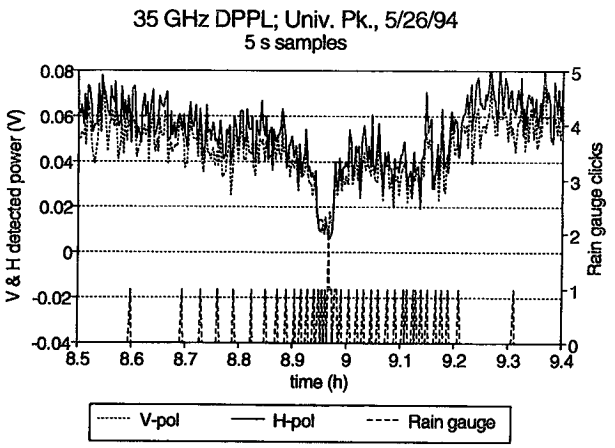

FIG. 3. Time series of vertical and horizontal received power and tipping-bucket-derived rain rate during a rain event at University Park, Pennsylvania. The tipping bucket was located at one end of the propagation link. The 5-s samples by the tipping-bucket result in highly quantized estimates of rain rate. Note the strong attenuation at both polarizations during the period of heavy rain. Also note that the vertically polarized signal is slightly less attenuated.

suggested by the standard deviation of P_{avg} at 500-min integration time. In contrast, the observed level of ΔP remained steady at the 0.01-dB level, which is consistent with its 500-min standard deviation. These results suggest that, using differential processing, the DPPL can estimate rain rate with about 0.5 mm h^{-1} absolute accuracy. The precision of these estimates will vary with integration time according to Figure 2b. For example, 5-s samples will result in a precision of ± 10 mm h^{-1}, 5-min averages in a precision of ± 1 mm h^{-1}.

5. Demonstration of differential attenuation in rain

The DPPL was deployed during most of the spring and summer of 1994 in the configuration described above for the stability test. As noted above, the line of sight path between the DPPL and corner reflector was unobstructed. In addition, the volume of space centered on the reflector and within several range bins along the axis of the antenna beam and within several beamwidths across the axis was occupied only by the reflector and the chimney. The power received from the chimney itself could be significant if changes in its differential radar cross section were correlated with the rain (e.g., by preferentially oriented wetting). However, the power received from the chimney was approximately 20 dB below that received from the corner reflector, so this contribution to the signal was considered minor.

Ground truth of the rain rate was provided by a standard "tipping bucket" located at the DPPL end of the propagation link. Two qualifications should be noted regarding an intercomparison between the DPPL and tipping-bucket data. The bucket records rain accumulation in 0.1-mm increments, and so provides fairly poor time resolution of the rain rate in light rain conditions. In addition, any nonuniformity in the spatial distribution of the rain rate would decorrelate point-by-point time samples by the two instruments. Both of these qualifications suggest that intercomparisons of time-averaged data may be more meaningful from the perspective of verifying DPPL performance. In fact, our analysis thus far indicates that there is considerably more scatter between point-by-point time samples of differential attenuation, on the part of the DPPL, and rain rate, on the part of the tipping bucket, than there is between the time-averaged data. Of course, this increased scatter likely contains useful information about the spatial correlation structure of the rain-rate distribution. This is one area of ongoing investigation by the authors.

A time series of 5-s samples of the vertical and horizontal received power during one rain event is shown in Fig. 3, together with the rain gauge measurements made by the tipping bucket. A 0.1-mm accumulation of rain during any one 5-s sampling interval corresponds to one rain gauge "click." The DPPL data clearly indicates a large decrease in both P_h and P_v during the time period 8.9–9.0 h. The magnitude of this decrease is generally consistent with the relationship described by (2). The differential behavior of the attenuation is more easily seen by considering the ratio of the two received powers. This ratio is shown in Fig. 4 before any time averaging of the raw 5-s samples. The highest differential attenuation, 5.6 dB, coincides with the only sample of the tipping bucket that recorded 0.2 mm of accumulation in a 5-s period (all other accumulations being either 0.0 or 0.1 mm). An estimate of the time series of the rain-rate results from averaging the tipping-bucket data and noting that a 0.1-mm accumulation over 5 s corresponds to an instantaneous

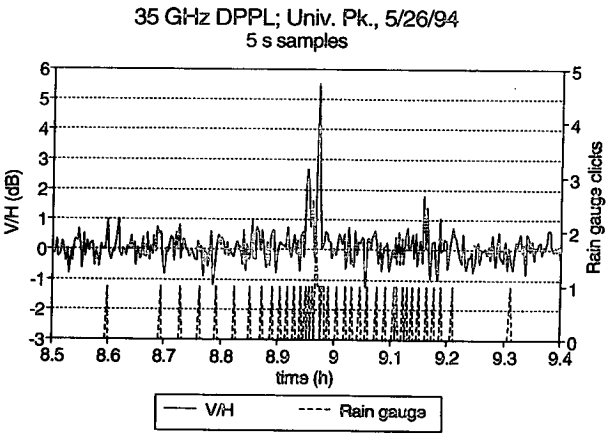

FIG. 4. The 5-s sampled time series of the differential attenuation ΔA. Note that the highest recorded differential attenuation of 5.6 dB coincides with the sole instance of 0.2-mm accumulation during a 5-s period.

rain rate of 72 mm h^{-1}. A 1-min running average of the data shown in Fig. 4 is plotted in Fig. 5. Note that although the tipping-bucket time series can now be interpreted in terms of rain rate, the smoothed DPPL data has lost its extremely high values of ΔA; the highest value has been reduced from 5.6 to 1.5 dB. This large reduction suggests that a downpour lasting considerably less than 1 min occurred at this time. This is consistent with the single 0.2-mm accumulation recorded by the tipping bucket over a 5-s interval during the same period of time.

A scatterplot of ΔA and R from Fig. 5 is shown in Fig. 6. A linear regression of these data provides an estimate of the measured sensitivity of ΔA to R over this 255-m (one way) range, corresponding to the model sensitivity given by (3) for a 1-km pathlength. After normalizing the measured sensitivity to a 1-km path, the result is

$$\Delta A_{\mathrm{DPPL}} = 0.035R. \qquad (4)$$

It should be emphasized that this result is preliminary. For example, the regression assumes a linear relationship between ΔA and R over the full range of values, whereas Fig. 6 indicates a difference in the sensitivity of ΔA to R at low (0–25 mm h^{-1}) and at high (25–50 mm h^{-1}) rain rates. For comparison, the sensitivity relations indicated by (3) and (4) are also shown in Fig. 6. Note that both (3) and (4) suggest a higher sensitivity than the data indicates at low rain rates and a lower sensitivity than the data indicates at high rain rates. There are a number of issues, other than rain drop ellipticity, that may be contributing to this behavior. They include multiple scattering, raindrop canting (Beard and Jameson 1983), and raindrop oscillation

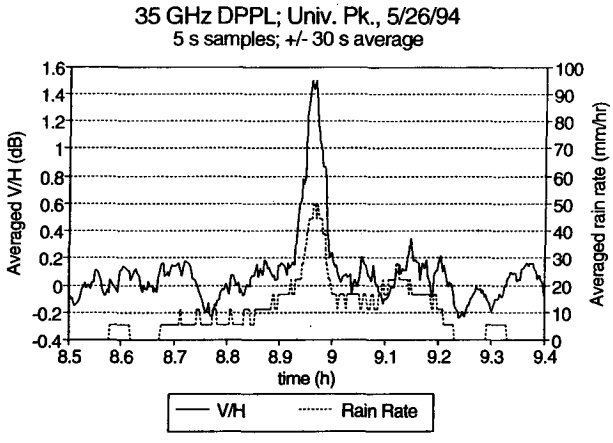

FIG. 5. Running time average of the data in Fig. 4, with a ±30-s rectangular averaging window. The averaging is necessary to extract a meaningful time series of rain rate from the highly quantized raw tipping-bucket data. However, the very high values of differential attenuation present in the 5-s sampled DPPL data are lost here. This suggests that a very heavy downpour occurred lasting considerably less than 1 min.

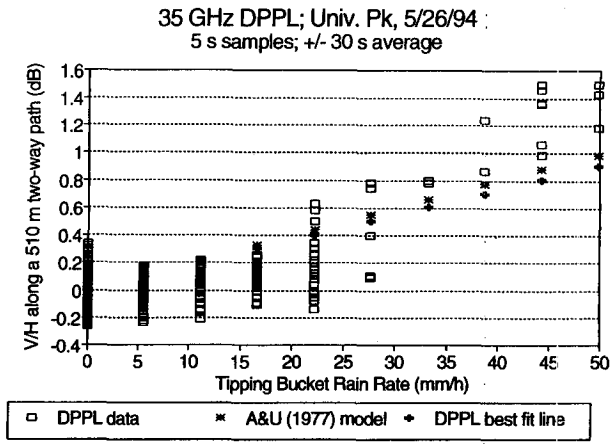

FIG. 6. Scatterplot of the smoothed DPPL and tipping-bucket data shown in Fig. 5. The slope of this plot is an indication of the sensitivity of differential attenuation to rain rate over a 510-m two-way path. However, there are numerous sources of spatial and temporal decorrelation between the two datasets due to their sampling characteristics. This estimate of sensitivity should be considered a preliminary and qualified confirmation of the modeled sensitivity given by Eq. (3) in the text. For comparison, the sensitivity predicted by Atlas and Ulbrich (1977) and by a linear regression fit of this data are also shown.

(Beard 1984). However, any interpretation of this dataset must also keep in mind the sampling problems with the tipping bucket that were discussed above. Recall that the sampling becomes especially problematic in very light rain conditions. Furthermore, the relative precision of the DPPL measurement of ΔA is reduced in light rain because, while ΔA is lower, the instrument noise is largely independent of rain rate. For these reasons, we defer any more selective processing of this data until a more reliable, and significantly larger, database is assembled. Instead, these results should simply be considered as a preliminary and qualitative demonstration of the DPPL.

6. Conclusions and discussion

The design and initial performance of the dual-polarization propagation link has been presented. The basic design of the DPPL is that of a small, low-cost, low-power, portable, dual linearly polarized pulsed radar. The DPPL operates at 35 GHz in order to reduce the dependence of its attenuation through rain on the size distribution and temperature of the rain drops. It operates in a differential attenuation mode and at a fairly high polarization switching speed of 2200 Hz in order to cancel instrumental- and range-induced fluctuations in the processed data. Differential attenuation processing also reduces the dependence of the rain-rate estimates on changes in the ellipticity of the raindrop shape with rain rate. The link path is bidirectional, with both the transmit and receive electronics at one end and a corner reflector at the other. This approach significantly

simplifies deployment logistics relative to a unidirectional link since the corner reflector is passive.

Initial measurements by the DPPL indicate that there is a clear differential attenuation response versus rain rate. "Ground truth" of the rain rate was provided by a tipping bucket located at one end of the propagation link. Use of a tipping bucket introduces considerable uncertainty into the intercomparison analysis. The rain-rate time series provided by the bucket is highly quantized and is only a point measurement, as opposed to the spatial average sensed by the DPPL. Both of these limitations could be relaxed somewhat by intercomparison with an array of optical range gauges deployed along the link path. This is an area of ongoing investigation by the authors.

There are a number of other deployment scenarios with the DPPL that the authors are also considering. Range gating of multiple corner reflectors along the link path will permit measurement of the differential range attenuation, similar to the systems discussed in Wallace (1988). It is expected that a differential range measurement of A_{avg} will combine the benefits of the differential cancellation of instrument fluctuations demonstrated here for ΔA with the increased sensitivity to rain indicated by (2). The increase in sensitivity should be particularly helpful in very light rain conditions. All of these benefits would be realized while still retaining the insensitivity to variations in the raindrop shape. Another possible arrangement locates the DPPL at the center of a set of link paths viewed as "spokes of a wheel," each terminated by a corner reflector. The DPPL antenna beam could be directed straight up and then redirected to the horizontal by a rotating flat reflector. This type of arrangement would permit two-dimensional spatial averaging of the rain-rate distribution, for a more spatially correlated intercomparison with satellite estimates, for example, from TRMM. One other substantially more elaborate scenario would involve a suite of DPPL transceivers together with a number of corner reflectors deployed along two separated lines. The set of attenuation measurements from each transceiver to each reflector would comprise the projection functions needed to produce a tomographic two-dimensional image of the rain-rate distribution over the region bounded by the two lines. It is worth noting that such an image would probably contain useful information about the spatial structure of the rain only if the pathlengths were considerably longer than those measurable by the current DPPL hardware (of the order of tens of kilometers rather than 1 km). However, there are a few relatively straightforward upgrades to our instrument that would significantly increase its range of operation. These are also areas of ongoing investigation by the authors.

REFERENCES

Atlas, D., and C. W. Ulbrich, 1977: Path- and area-integrated rainfall measurements by microwave attenuation in the 1–3-cm band. *J. Appl. Meteor.*, **16**, 1322–1331.

Beard, K. V., 1984: Raindrop oscillations: Evaluation of a potential flow model with gravity. *J. Atmos. Sci.*, **41**, 1765–1774.

——, and A. R. Jameson, 1983: Raindrop canting. *J. Atmos. Sci.*, **40**, 448–454.

Collis, R. T. H., and M. G. H. Ligda, 1961: A radar raingauge. Preprints, *Ninth Radar Meteorology Conf.*, Kansas City, MO, Amer. Meteor. Soc., 391–395.

Crane, R. K., 1971: Propagation phenomena affecting satellite communication systems operating in the centimeter and millimeter wavelength bands. *Proc. IEEE*, **59**, 173–188.

Godard, S., 1965: Proprietes de l'attenuation par la pluie des ondes radioelectriques dans la bande 0.86 cm. *J. Rech. Atmos.*, **2**, 121–167.

Harrold, T. W., 1967: The attenuation of 8.6-mm wavelength radiation in rain. *Proc. Inst. Electr. Eng.*, **114**, 201–203.

Hogg, D. C., and T.-S. Chu, 1975: The role of rain in satellite communications. *Proc. IEEE*, **63**, 1308–1331.

Jameson, A. R., 1991: A comparison of microwave techniques for measuring rainfall. *J. Appl. Meteor.*, **30**, 32–54.

Mathur, S., 1994: 35 GHz dual polarization propagation link. M.S. thesis, Department of Electrical Engineering, The Pennsylvania State University, University Park, PA, 90 pp.

NASA, 1994: Tropical Rainfall Measuring Mission (TRMM) science. NASA Research Announcement NRA 94-MTPE-01, 22 pp.

Ruf, C. S., K. Aydin, and S. Mathur, 1994: Rain rate estimation from attenuation measurements using a 35 GHz dual polarization propagation link. *Proc. 1994 Int. Geoscience Remote Sensing Symp.*, Pasadena, CA, IEEE, 1777–1779.

Ryde, J. W., 1947: The attenuation and radar echoes produced at centimeter wavelengths by various meteorological phenomena. *Meteorological Factors in Radio Wave Propagation*, Physical Society of London, 169–189.

Wallace, H. B., 1988: Millimeter-wave propagation measurements at the Ballistic Research Laboratory. *IEEE Trans. Geosci. Remote Sens.*, **26**, 253–258.

Wexler, R., and D. Atlas, 1963: Radar reflectivity and attenuation of rain. *J. Appl. Meteor.*, **2**, 276–280.